7B.1 Ka and X-band Radar Observations of Multiple Rear-Flank Downdraft Surges and an Intense Near-Surface Vortex on 18 May 2010

Patrick S. Skinner*, Christopher C. Weiss,
Texas Tech University, Lubbock, Texas
Michael M. French, Howard B. Bluestein,
The University of Oklahoma, Norman, Oklahoma,
I. PopStefanija,
ProSensing, Inc., Amherst, Massachusetts
and R. Bluth
Naval Postgraduate School, Monterey, California

1. Introduction

The instrument armada participating in the second Verification of the Origin of Rotation in Tornadoes Experiment (VORTEX2) targeted a pretornadic, high-precipitation supercell west of Dumas, Texas on 18 May 2010. Datasets collected on the Dumas storm include a long-duration, short-baseline dual-Doppler deployment by two 35 GHz, Ka-band mobile radars operated by Texas Tech University (TTUKa) (Weiss et al. 2009) overlapping with a long-term deployment of the X-band, electronically-steered MWR-05XP radar fielded by the University of Oklahoma, ProSensing, Inc., and The Naval Postgraduate School (Bluestein et al. 2010).

The TTUKa Doppler radars employ a narrow, 0.49° beamwidth coupled with nonlinear pulse compression techniques to obtain an azimuthal and range gate spacing of approximately 35 m for pulse lengths less than or equal to 20 μs[1]. The baseline of the TTUKa dual-Doppler deployment on the Dumas supercell was 3.3 km (Fig. 1), which combined with 0.0° elevation sector scans, provides a representation of the near-surface kinematics of the Dumas mesocyclone with a high spatial and temporal resolution. The limited data collection in the vertical of the TTUKa radars, which did not scan above 0.5° for the Dumas deployment, is complemented by the complete volume scans (1-40° in elevation) of the MWR-05XP. The MWR-05XP utilizes a combination of mechanical and electronic beam steering to collect a full volume of data roughly every 10 seconds for scanning strategies implemented in VORTEX2. The high temporal resolution and greater range of data collected by the MWR-05XP provides storm-scale horizontal and vertical context for TTUKa dual-Doppler syntheses.

The dual-Doppler analysis of TTUKa data reveal a complex and rapidly-evolving rear-flank downdraft (RFD) within the Dumas supercell, with three distinct internal RFD surges developing and merging over a period of roughly 10 minutes and a brief, intense near-surface vortex developing north of the apex of the final internal surge. The internal surges coincide with an intensification of a low-level mesocyclone removed in the vertical from a persistent mid-level mesocyclone in MWR-05XP data, which is qualitatively similar to the process in which three-dimensional numeric simulations produce shallow occlusion downdrafts through a downward-directed vertical pressure gradient force (Wicker and Wilhelmson 1995; Adlerman et al. 1999).

2. Methodology

Significant quality control of raw data from both the TTUKa and MWR-05XP radars is required prior to analysis. Initially, each sweep is reoriented such that a 0° azimuth corresponds to true north. This is accomplished by overlaying known positions of man-made structures such as power poles or tall towers on each radar sweep; the sweep is then rotated to match observed ground clutter patterns with known targets. This technique has the additional benefit of removing "jitter" present in sector scans due to post-processing software and antenna acceleration errors. After the heading of each sweep has been corrected, a series

* *Corresponding author address:* Patrick Skinner, Texas Tech University, Wind Science and Engineering Research Center, 10^{th} and Akron, Lubbock, TX 79409.
E-mail: patrick.skinner@ttu.edu

[1] A pulse length of 20 μs requires a 1 km blanking region from the radar before usable data can be obtained.

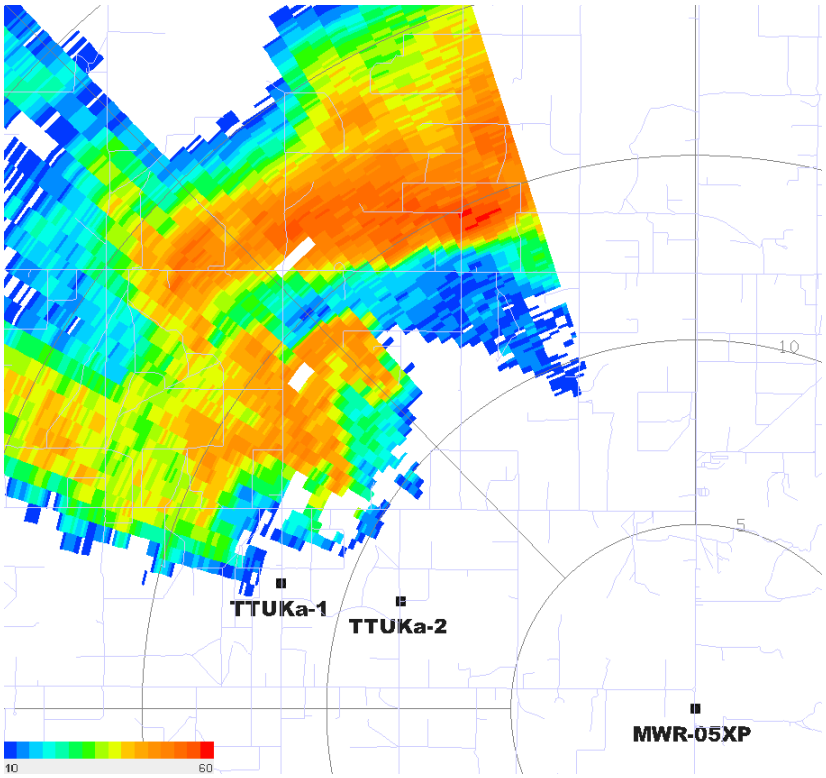

FIG. 1. Positions of TTUKa-1, TTUKa-2, and MWR-05XP mobile radars for pertinent deployments on the Dumas supercell. Positions are overlayed with MWR-05XP 1.0° elevation reflectivity (dBZ) at 2300 UTC and regional road network. Range rings are plotted every 5 km centered at location of the MWR-05XP.

of quality assurance procedures are performed using the SOLO and DREADER radar processing software available from the National Center for Atmospheric Research (NCAR) and Earth System Research Laboratory (ERSL), respectively. Incoherent values of uncalibrated reflectivity factor (reflectivity) and radial velocity are removed by thresholding data below 2.5 dBZ for both the TTUKa and MWR-05XP radars[2], ground clutter is removed and radial velocities are dealiased in SOLO, and glitching and speckling are removed through automated procedures in DREADER. Finally, range-folding and other gates subjectively determined to be erroneous are manually corrected.

After quality assurance has been completed, both TTUKa and MWR-05XP data are objectively analyzed using a two-pass exponential filter as in Majcen et al. (2008). The Barnes smoothing parameter (κ) is calculated as $1.33 \cdot \mu$ as in Pauley and Wu (1990) with μ representing the coarsest spatial resolution of data included in objective analysis (Trapp and Doswell 2000) and is equal to $R_{max} \cdot \theta$ where R_{max} is the maximum range from the radar and θ is the angular beamwidth. Values of μ were selected to maximize the retention of small-wavelength features in objective analysis (Table 1) with R_{max} corresponding to the limit of the dual-Doppler domain for a 30° crossing angle for TTUKa data and the minimum value at which the entirety of the Dumas mesocyclone was sampled for MWR-05XP data. Resulting objective analyses achieve a 50% Barnes response for wavelengths of approximately 150m(1500m) for TTUKa(MWR-05XP) observations (Fig. 2). Dual-Doppler synthesis of 0° elevation sweeps of TTUKa data allow for the two-dimensional wind field to be calculated without solving for vertical velocity through integration of the mass continuity equation.

[2]MWR-05XP sweeps above 10° elevation angles are thresholded at 5 dBZ to remove excessive speckling.

3. Analysis

a. TTUKa

Dual-Doppler syntheses of TTUKa data reveal considerable heterogeneity and transient features within the Dumas RFD (Figs. 3, 4). At the inception of the deployment at 2256 UTC (all times hereafter in

TABLE 1. Objective analysis settings for 18 May 2010 data.

Value	TTUKa	MWR-05XP
R_{max}	6.37 km	20.0 km
μ	0.0545 km	0.628 km
κ	0.00525 km^2	0.698 km^2
Convergence Parameter (γ)	0.3	0.3
Grid Spacing (Δ)	25 m	250 m
Radius of Influence	150 m	1000 m

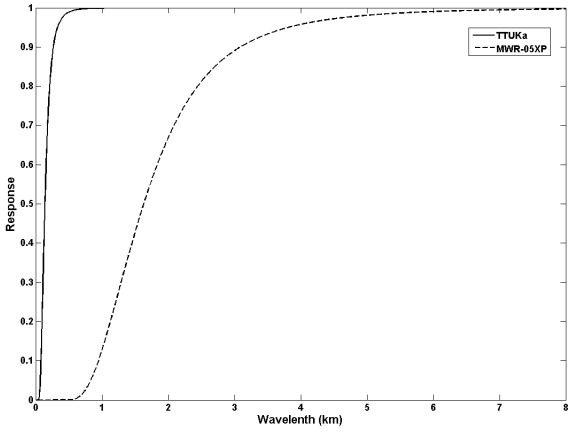

FIG. 2. Barnes response function values for TTUKa (solid) and MWR-05XP (dashed) objective analyses.

UTC) the primary RFGF is apparent as a relatively broad convergence zone associated with a wind shift from southeasterly to southwesterly across the eastern portion of the dual-Doppler domain. The trailing broad RFD is fairly homogeneous with wind speeds varying from 10 - 20 m s^{-1} (Fig. 3a). The first internal RFD surge (surge A) enters the western portion of the domain approximately 90 seconds after the initial analysis with the initial RFGF only subtly evident at the extreme eastern edge of the analysis (Fig. 3b). Surge A is initially compact, with a width of approximately 2 km and exhibits wind speeds much greater than the surrounding broad-scale RFD, upwards of 50 m s^{-1}. However, surge A rapidly expands and decelerates over the next 90 seconds and by 2259 is roughly 3 km in width with only a small area of wind speeds exceeding 35 m s^{-1} (Fig. 3c). There is evidence of the leading edge of a second internal RFD surge in the 2259 analysis (surge B), which becomes much more pronounced by 2301 with maximum wind speeds greater than 40 m s^{-1} and broad cyclonic curvature in the wind field north of the surge apex (Fig. 3d). This curvature tightens into a broad, closed circulation trailing the apex of surge B at 2302 (Fig. 4a). Surge B has continued to decelerate as it expands and is merging with the remnants of surge A at 2303:26 (Fig. 4b). A narrow third internal RFD surge (surge C) wraps cyclonically around the low-level circulation over the following 45 seconds coincident with a rapid intensification of near-surface rotation (Fig. 4b, c). At 2304 the small, intense vortex just north of the apex of surge C exhibits maximum shear greater than 75 m s^{-1} and is coincident with a spiraling reflectivity band and low-reflectivity "eye" in single-Doppler data suggesting that it could be interpreted as a tornado. However, the extremely short duration of the vortex, which only maintains shear values greater than 40 m s^{-1} for two sector scans (24 seconds) fails to meet the prescribed criteria for tornadoes observed by mobile Doppler radars employed by Alexander and Wurman (2008) and has led to a classification of this vortex as nontornadic. The rapid dissipation of the near-surface vortex is apparent in the 2305 analysis, where only a broad, weak cyclonic circulation persists to the northwest of the single internal RFGF representing the merger of surges A, B,

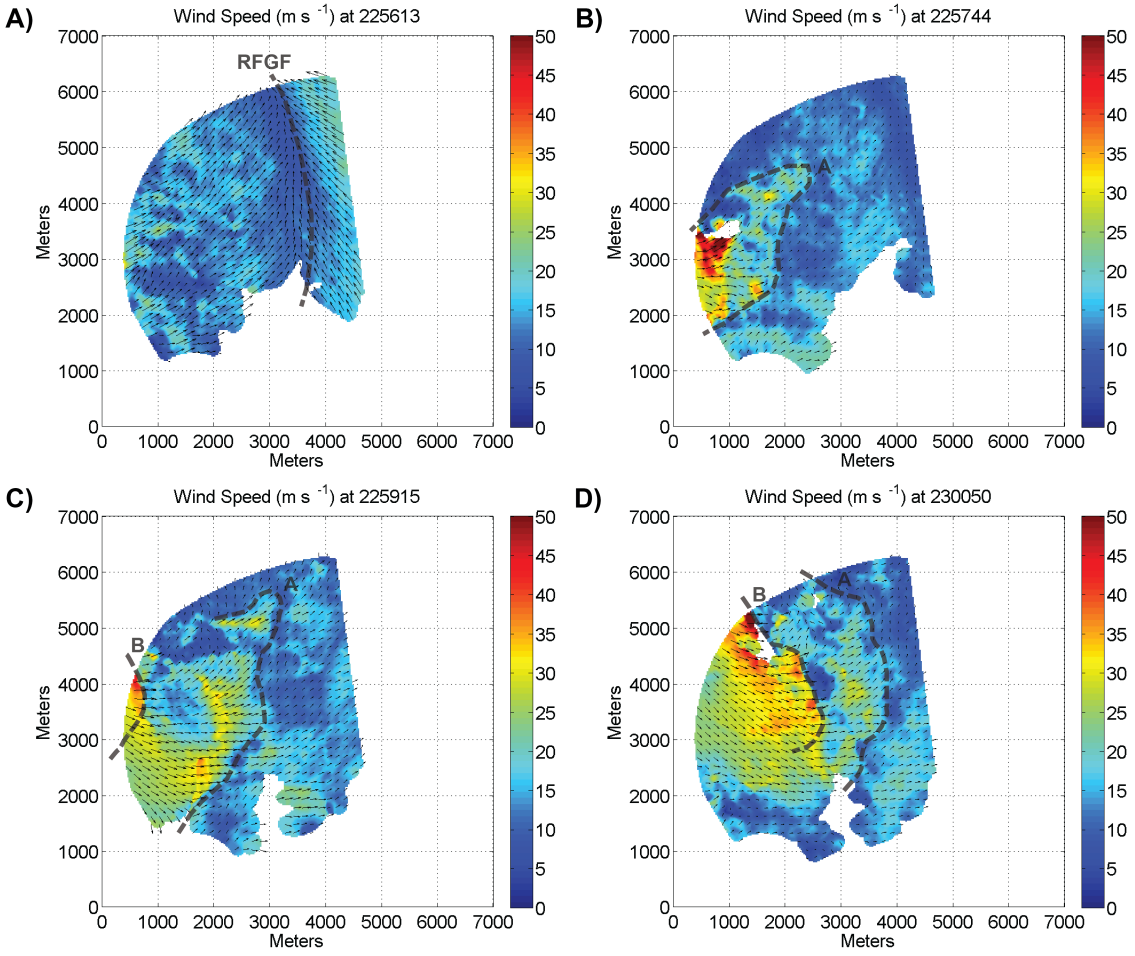

FIG. 3. TTUKa dual-Doppler analyzed wind vectors (magnitude shaded in m s^{-1}) in the Dumas supercell at (a) 2256:13, (b) 2257:44, (c) 2259:20, and (d) 2300:50 UTC. Kinematic boundaries are indicated by heavy dashed lines with "RFGF" indicating passage of the initial RFD gust front and letters representing internal RFD surge gust fronts.

and C (Fig. 4d).

b. MWR-05XP

Objectively analyzed MWR-05XP data can be viewed in three dimensions utilizing the Visualization and Analysis Platform for Ocean, atmosphere, and solar Researchers (VAPOR) software developed by NCAR (Clyne et al. 2007) (Figs. 5-7). Horizontal wind shear within the Dumas storm is calculated for each gridpoint by subtracting the radial velocity from each surrounding gridpoint within a 1.5 km radius and assigning the maximum magnitude of wind shear found to the target gridpoint. This calculation results in the strongest regions of cyclonic velocity couplets being represented by areas of negative wind shear (cool colors) residing southwards of regions of positive wind shear (warm colors).

A strong, deep, and persistent mid-level mesocyclone is present in the Dumas supercell during the early portions of the MWR-05XP deployment, with only weak rotation present below 2 km above ground level (AGL) (Fig. 5b). The mid-level mesocyclone weakens and contracts by 2255 (Fig. 5d) and exhibits a strong tilt from south (low-levels) to north (upper levels) with a maximum intensity centered between 2.5 and 5 km AGL. Modest reintensification of the mid-level mesocyclone occurs over the following four minutes and by 2259 a compact area of strong rotation is present between 2.5 and 4 km AGL (Figs. 5d, 6b). During this time an area of near-surface cyclonic rotation distinct from the mid-level mesocyclone begins to intensify and by 2300 (Fig. 6d)

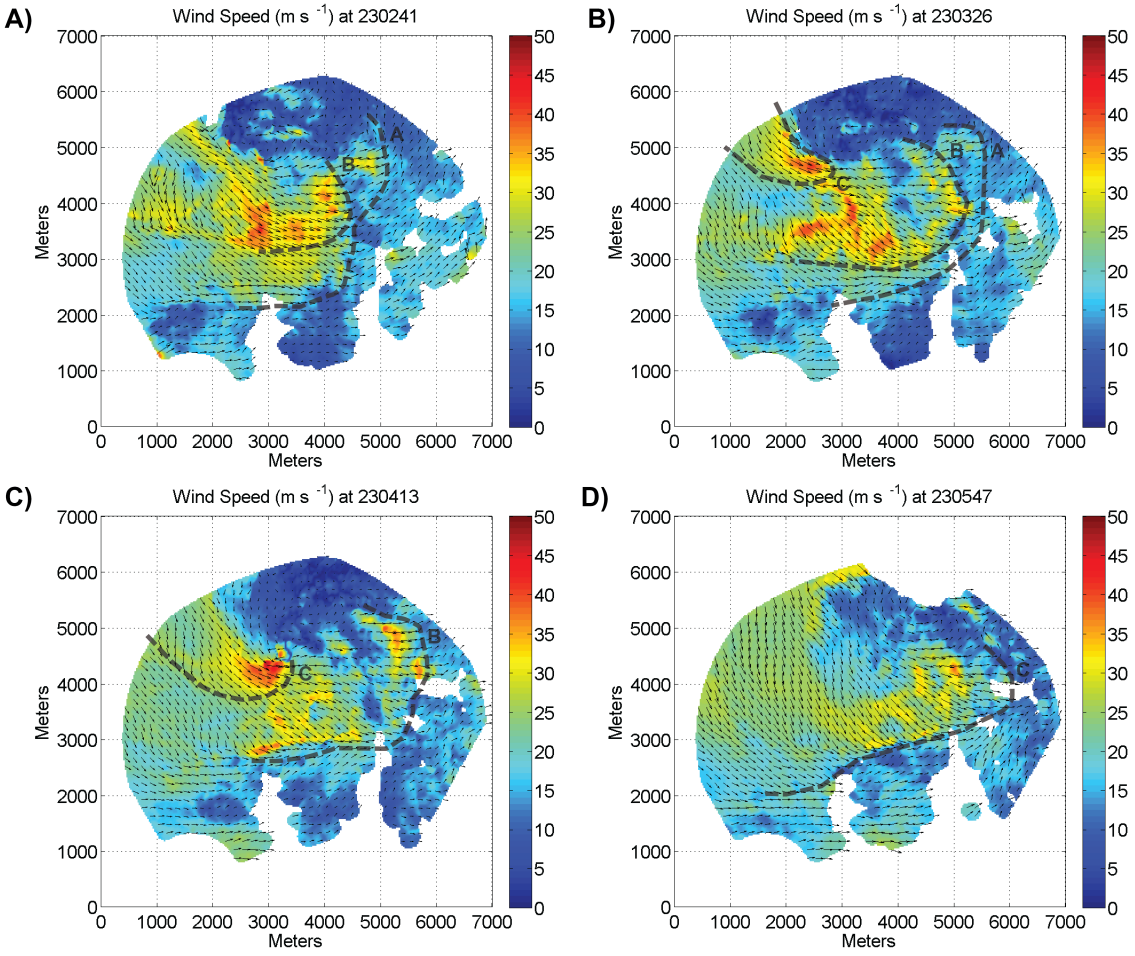

FIG. 4. Same as Fig. 3 except for (a) 2302:41, (b) 2303:26, (c) 2304:13, and (d) 2305:47 UTC.

exhibits a roughly 1 km deep layer of horizontal wind shear greater than 25 m s^{-1}. It is noteworthy that the timing and position of low-level mesocyclone intensification in MWR-05XP data coincides with the development of internal surge B in TTUKa dual-Doppler syntheses. After 2300 the most intense portion of the mid-level mesocyclone begins to advect upwards and weaken (Figs. 6f, 7). The low-level mesocyclone initially maintains its intensity during this period (Fig. 6f) before weakening as it becomes farther displaced in the vertical and horizontal from the axis of maximum rotation in the mid-level mesocyclone (Fig. 7). Only weak cyclonic rotation is observed below 5 km AGL at 2304 (Fig. 7d), which coincides with the maximum intensity of the near-surface vortex in TTUKa data. However, the scale of the vortex in TTUKa analyses is approximately 300 m (Fig. 4c), which is well below the minimum wavelength retained by objective analysis of MWR-05XP data (Fig. 2).

The three-dimensional renders of reflectivity reveal structure similar to what is expected in a supercell thunderstorm with a pronounced weak echo overhang and a hook-echo wrapping cyclonically around the mid-level updraft (Lemon and Doswell 1979). There is no evidence of a descending reflectivity core (DRC) originating from atop the weak echo overhang (Rasmussen et al. 2006; Byko et al. 2009) through the entirety of the deployment. However, there is a subtle intensification of reflectivity values at the leading edge of the hook echo originating from the low levels of the hook echo during the 2259 - 2300 time period (Figs. 6a, c). Though it does not meet their qualifications for a DRC, this intensification shares similarities with Type III DRCs defined by Byko et al. (2009) and associated with the development of an occlusion downdraft.

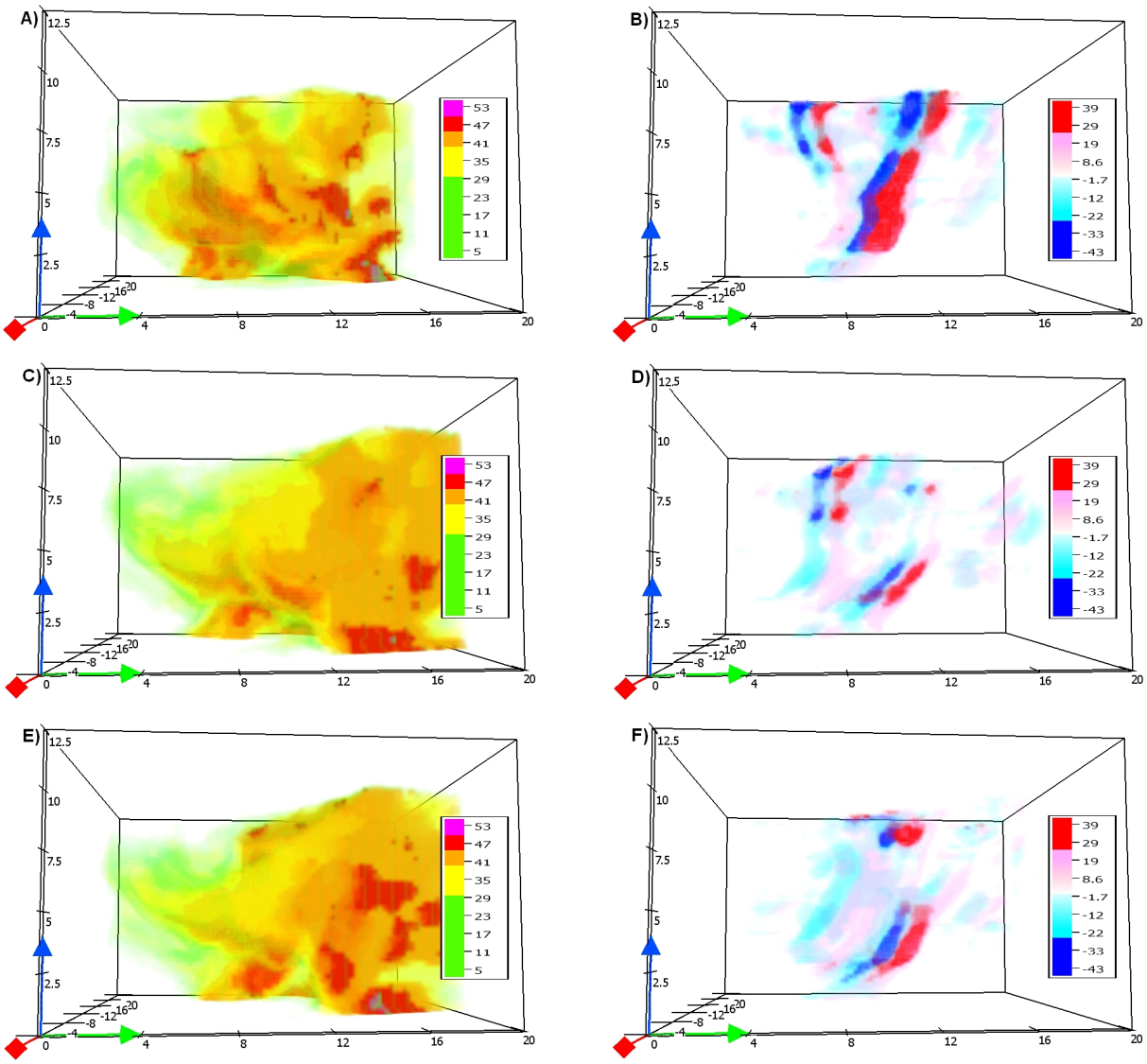

FIG. 5. Three-dimensional renders of (a, c, e) MWR-05XP reflectivity (dBZ) and (b, d, f) horizontal wind shear (m s^{-1}) for 2252:39 (a, b), 2255:43 (c, d), and 2257:55 (e, f) UTC. Red, green, and blue vectors denote the x, y, and z axes, respectively, which are labeled in km. View is from roughly east of the storm.

4. Discussion

The proliferation of mobile Doppler radar and in situ observing system deployments over the past 15 years has allowed fine-scale features such as internal RFD surges to be identified with increasing frequency (Finley and Lee 2004; Lee et al. 2004; Wurman et al. 2007; Marquis et al. 2008; Finley et al. 2010; Kosiba et al. 2010a,b; Lee et al. 2011; Marquis et al. 2011). Internal RFD surges and associated rear-flank gust fronts (RFGF) have been implicated in tornadogenesis (Finley et al. 2010; Kosiba et al. 2010b), tornado maintenance (Marquis et al. 2008; Finley et al. 2010; Kosiba et al. 2010a; Marquis et al. 2011), and tornado demise (Finley et al. 2010). Parcel trajectories from dual-Doppler syntheses have shown that air parcels from within an internal RFD enter the low-level mesocyclone and tornado (Kosiba et al. 2010a,b), convergence along an internal RFGF can assist with tornado maintenance (Marquis et al. 2011), and internal RFDs can exhibit differing buoyancy characteristics than the broad-scale RFD and storm environment (Finley and Lee 2004; Lee et al.

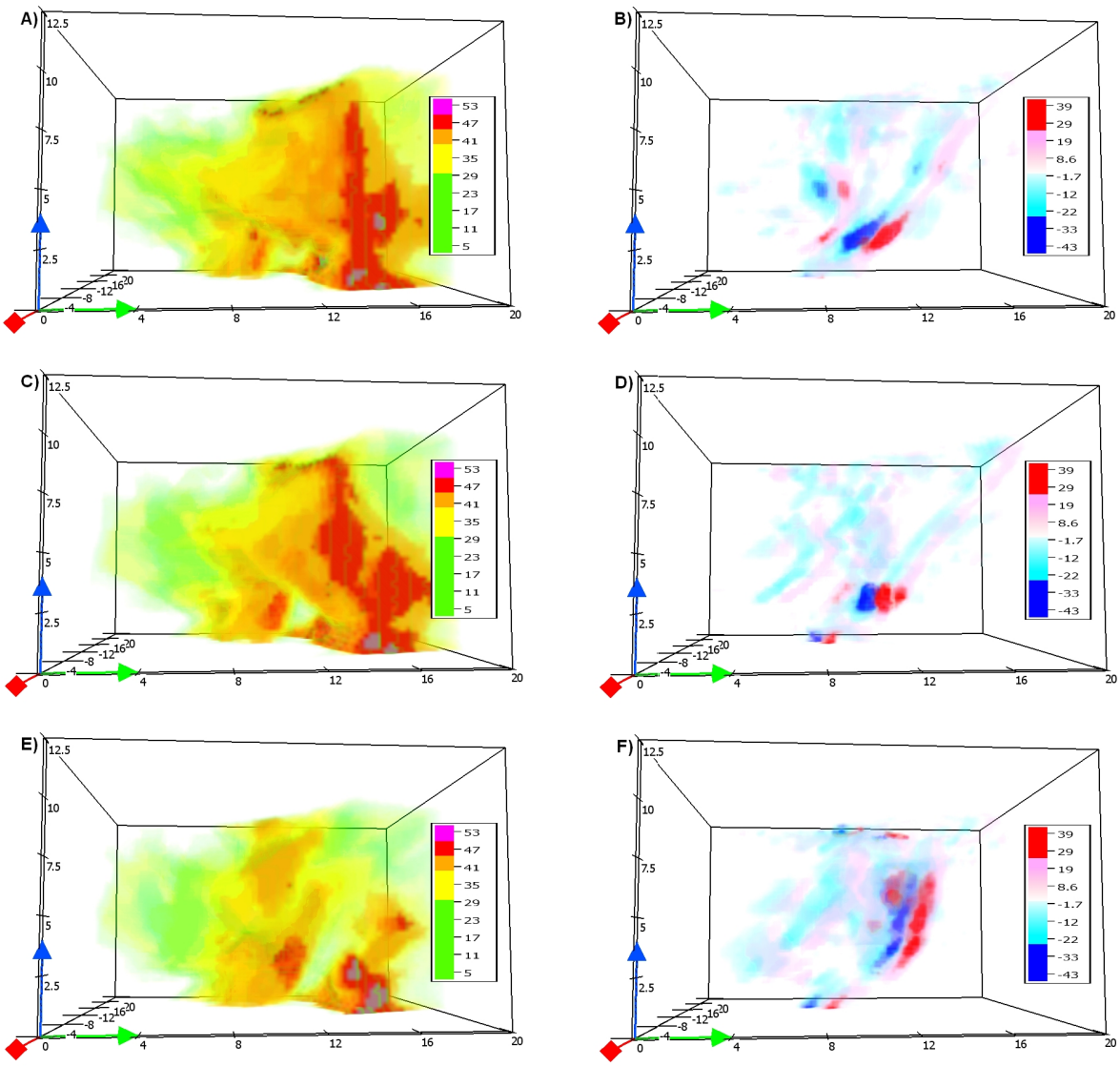

FIG. 6. Same as Fig. 5 except for 2259:38 (a, b), 2300:54 (c, d), and 2302:38 (e, f) UTC.

2004; Finley et al. 2010; Lee et al. 2011; Marquis et al. 2011).

Data presented herein documents three internal RFD surges during the pretornadic phase of the Dumas supercell. The RFD surges develop and merge into a single internal RFGF over the course of ten minutes with the final surge developing an intense, brief, near-surface vortex just north of its apex (Figs. 3, 4). The evolution of the second internal RFD surge coincides with an intensification of the low-level mesocyclone as observed in MWR-05XP data (Figs. 5-7). The low-level mesocyclone begins to intensify as it propagates underneath the axis of a mid-level mesocyclone with maximum rotation between 2.5 and 4 km AGL and weakens as the mid-level mesocyclone advects upward and becomes farther displaced to the north of the low-level mesocyclone.

Development of the low-level mesocyclone in MWR-05XP data qualitatively follows the evolution of low-level mesocyclone intensification through an upward-directed vertical pressure gradient force produced in numeric simulations (Wicker and Wilhelmson 1995; Adlerman et al. 1999) and dual-Doppler studies (Dowell and Bluestein 2002) where a rotationally induced pressure deficit in the mid-level mesocyclone triggers an upward-directed vertical pressure

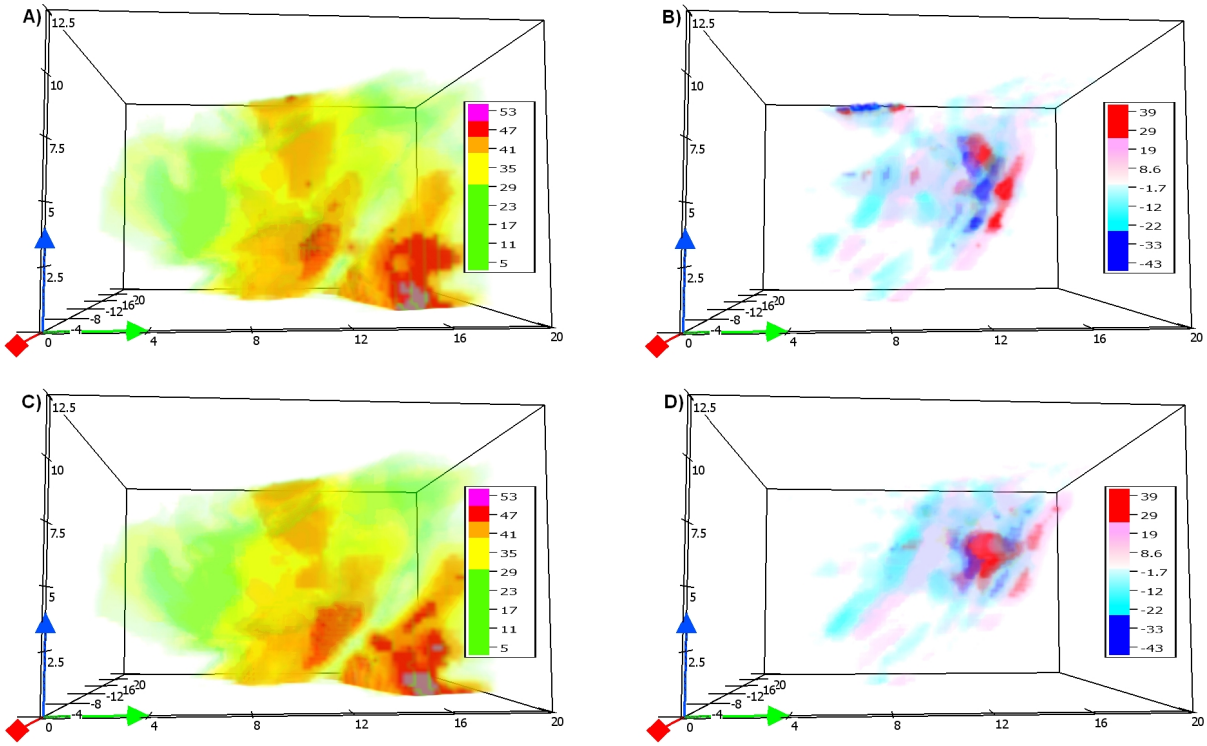

FIG. 7. Same as Fig. 5 except for 2303:26 (a, b) and 2304:13 (c, d) UTC.

gradient force at lower levels, increasing vertical velocity and enhancing the stretching of vertical vorticity, resulting in an intensification of the low-level mesocyclone. The intensification of vertical vorticity within the low-level mesocyclone to levels above those in the mid-level mesocyclone, as is observed in MWR-05XP data, induces a second, downward-directed vertical pressure gradient force near the surface resulting in an occlusion downdraft (Klemp and Rotunno 1983; Wicker and Wilhelmson 1995; Adlerman et al. 1999; Wakimoto and Cai 2000). The development of internal RFD surges in the Dumas supercell coincident in time and space with an intensification of the low-level mesocyclone suggests that it is possible the internal RFD surges observed are the surface manifestation of an occlusion downdraft originating within the low-level mesocyclone. Though not explicitly identified as an internal RFD surge, Markowski (2002) defined the surface representation of an occlusion downdraft as "a rapid, small-scale intensification of the RFD that occurs after the RFD transports larger angular momentum toward the ground", which aptly describes the internal RFD surges observed in the Dumas storm.

The genesis of the intense, near-surface vortex north of the apex of an internal RFD surge (Fig. 4c) is similar to cases described by Kosiba et al. (2010b) and Marquis et al. (2011). Enhanced convergence into a vortex pendant to an internal RFGF has been shown to promote the maintenance of near-surface vertical vorticity (Marquis et al. 2011). However, the transient nature of the vortex observed in the Dumas storm suggests that conditions favorable for the maintenance of near-surface vertical vorticity were not present or very limited in duration. The vortex was observed to retrograde with respect to the leading edge of the internal RFGF of surge C shortly after intensification (Fig. 4d) potentially removing it from a source of low-level convergence and promoting dissipation. Additionally, the vortex developed in a location well removed from the center of the mid-level mesocyclone and at a time when mid-level rotation was weak, suggesting weaker vertical velocity within the storm updraft, which has been shown by Dowell and Bluestein (2002) to promote tornado dissipation. A final potential tornadogenesis failure mechanism for the Dumas storm would be buoyancy characteristics of surface air parcels which inhibited lifting to their level of free convection, reducing the amount of tilting of horizontal vorticity within the

RFD surge into the vertical and subsequent stretching (Markowski et al. 2002).

5. Summary and Future Work

Three internal RFD surges, with an intense, brief vortex pendant to the third surge, have been documented through analysis of dual-Doppler TTUKa and single-Doppler MWR-05XP data. The final two internal RFD surges develop coincident with an intensification of the low-level mesocyclone, which is consistent with conceptual models of occlusion downdraft development. The vortex north of the apex of the third internal RFD surge develops in a region of strong convergence pendant to the RFGF, but rapidly retrogrades with respect to the RFGF and is located at a large distance from the mid-level updraft, both of which are associated with tornado dissipation.

Incorporation of additional datasets available from VORTEX2 such as the Shared Atmospheric Research and Teaching Radar (SMART-R) (Biggerstaff et al. 2005), Doppler on Wheels (DOW) (Wurman et al. 1997), and mobile mesonet (Straka et al. 1996) will allow the storm-scale evolution, dual-polarization characteristics, and surface thermodynamics of the Dumas supercell to be explored. Quantitative assessment of the origin and forcing mechanisms of the broad-scale RFD and internal RFD surges within the Dumas storm will be possible through a series of Ensemble Kalman Filter (EnKF) data assimilation experiments using mobile Doppler radar observations.

Acknowledgments.

This research was supported by NSF grants AGS-0964088 to Texas Tech University and AGS-0821231 to the University of Oklahoma. The authors wish to thank Dr. Conrad Ziegler, Curtis Alexander, Anthony Reinhart, and Scott Gunter for their assistance with radar editing software. Dr. Brian Hirth and Dr. Sylvie Lorsolo provided helpful code for the objective analysis of radar data. Jerry Guynes, Dr. John Schroeder, Ryan Metzger, Amanda Thibault, Rich Krupar, and Trevor Boucher are acknowledged for their assistance with TTUKa data collection.

REFERENCES

Adlerman, E. J., K. K. Droegemeier, and R. Davies-Jones, 1999: A numerical simulation of cyclic mesocyclogenesis. *J. Atmos. Sci.*, **56**, 2045–2069.

Alexander, C. and J. Wurman, 2008: Updated mobile radar climatology of supercell tornado structures and dynamics. *Preprints, 24th Conf. Severe Local Storms*, Savannah, GA, Amer. Meteor. Soc., 19.4.

Biggerstaff, M. I., et al., 2005: The Shared Mobile Atmospheric Research and Teaching Radar: A collaboration to enhance research and teaching. *Bull. Amer. Meteor. Soc.*, **86**, 1263–1274.

Bluestein, H. B., M. M. French, I. PopStefanija, R. T. Bluth, and J. B. Knorr, 2010: A mobile, phased-array Doppler radar for the study of severe convective storms. *Bull. Amer. Meteor. Soc.*, **91**, 579–600.

Byko, P. M., Z., Y. Richardson, J. Wurman, and E. Adlerman, 2009: Descending reflectivity cores in supercell thunderstorms observed by mobile radars and in a high-resolution numerical simulation. *Weather and Forecasting*, **24**, 156–186.

Clyne, J., P. Mininni, A. Norton, and M. Rast, 2007: Interactive desktop analysis of high resolution simulations: application to turbulent plume dynamics and current sheet formation. *New J. Phys.*, **9**, 301.

Dowell, D. C. and H. B. Bluestein, 2002: The 8 June 1995 McLean, Texas, storm. Part II: Cyclic tornado formation, maintenance, and dissipation. *Mon. Wea. Rev.*, **130**, 2649–2670.

Finley, C. A. and B. D. Lee, 2004: High resolution mobile mesonet observations of RFD surges in the June 9 Basset, Nebraska supercell during Project ANSWERS 2003. *Preprints, 22nd Conf. on Severe Local Storms*, Hyannis, MA, Amer. Meteor. Soc., P11.3.

Finley, C. A., B. D. Lee, M. Grzych, C. D. Karstens, and T. M. Samaras, 2010: Mobile mesonet observations of the rear-flank downdraft evolution associated with a violent tornado near Bowdle, SD on 22 May 2010. *Preprints, 25th Conf. on Severe Local Storms*, Denver, CO, Amer. Meteor. Soc., 8A.2.

Klemp, J. B. and R. Rotunno, 1983: A study of the tornadic region within a supercell thunderstorm. *J. Atmos. Sci.*, **40**, 359–377.

Kosiba, K. A., J. Wurman, P. M. Markowski, Y. P. Richardson, D. C. Dowell, P. Robinson, and J. Marquis, 2010a: The Goshen County, Wyoming supercell of 5 June 2009 intercepted by VORTEX2: Tornado intensification phase. *Preprints, 25th Conf. Severe Local Storms*, Denver, CO, Amer. Meteor. Soc., 6.5.

Kosiba, K. A., J. Wurman, Y. P. Richardson, P. M. Markowski, D. C. Dowell, P. Robinson, and J. Marquis, 2010b: The Goshen County, Wyoming supercell of 5 June 2009 intercepted by VORTEX2: Tornadogenesis phase. *Preprints, 25th Conf. Severe Local Storms*, Denver, CO, Amer. Meteor. Soc., 6.4.

Lee, B. D., C. A. Finley, and T. M. Samaras, 2011: Surface analysis near and within the Tipton, Kansas tornado on 29 May 2008. *Mon. Wea. Rev.*, **139**, 370–386.

Lee, B. D., C. A. Finley, and P. S. Skinner, 2004: Thermodynamic and kinematic analysis of multiple RFD surges for the 24 June 2003 Manchester, South Dakota cyclic tornadic supercell during Project ANSWERS 2003. *Preprints, 22nd Conf. on Severe Local Storms*, Hyannis, MA, Amer. Meteor. Soc., P11.2.

Lemon, L. R. and C. A. Doswell, 1979: Severe thunderstorm evolution and mesocyclone structure as related to tornadogenesis. *Mon. Wea. Rev.*, **107**, 1184–1197.

Majcen, M., P. Markowski, Y. Richardson, D. Dowell, and J. Wurman, 2008: Multipass objective analysis of Doppler radar data. *J. Atmos. Oceanic Technol.*, **25**, 1845–1858.

Markowski, P. M., 2002: Hook echoes and rear-flank downdrafts: A review. *Mon. Wea. Rev.*, **130**, 852–876.

Markowski, P. M., J. M. Straka, and E. N. Rasmussen, 2002: Direct surface thermodynamic measurements within the rear-flank downdrafts of nontornadic and tornadic supercells. *Mon. Wea. Rev.*, **130**, 1692–1721.

Marquis, J., Y. Richardson, J. Wurman, and P. M. Markowski, 2008: Single- and dual-doppler analysis of a tornadic vortex and surrounding storm-scale flow in the Crowell, Texas, supercell of 30 April 2000. *Mon. Wea. Rev.*, **136**, 5017–5043.

Marquis, J., Y. P. Richardson, P. M. Markowski, D. C. Dowell, and J. Wurman, 2011: Tornado maintenance investigated with high-resolution dual-Doppler and EnKF analysis. *Mon. Wea. Rev.*

Pauley, P. M. and X. Wu, 1990: The theoretical, discrete, and actual response of the barnes objective analysis scheme for one- and two-dimensional fields. *Mon. Wea. Rev.*, **130**, 1692–1721.

Rasmussen, E. N., J. M. Straka, M. S. Gilmore, and R. Davies-Jones, 2006: A preliminary survey of rear-flank descending reflectivity cores in supercell storms. *Weather and Forecasting*, **21**, 923–938.

Straka, J. M., E. N. Rasmussen, and S. E. Fredrickson, 1996: A mobile mesonet for finescale meteorological observations. *J. Atmos. Oceanic Technol.*, **12**, 921–936.

Trapp, R. J. and C. A. Doswell, 2000: Radar data objective analysis. *J. Atmos. Oceanic Technol.*, **17**, 105–120.

Wakimoto, R. M. and H. Cai, 2000: Analysis of a nontornadic storm during VORTEX 95. *Mon. Wea. Rev.*, **128**, 565–592.

Weiss, C. C., J. L. Schroeder, J. Guynes, P. S. Skinner, and J. Beck, 2009: The TTUKa mobile Doppler radar: Coordinated radar and in situ measurements of supercell thunderstorms during Project VORTEX2. *Preprints, 34th Conf. on Radar Meteorology*, Williamsport, VA, Amer. Meteor. Soc., 11B.2.

Wicker, L. J. and R. B. Wilhelmson, 1995: Simulation and analysis of tornado development and decay within a three-dimensional supercell thunderstorm. *J. Atmos. Sci.*, **52**, 2675–2703.

Wurman, J., Y. P. Richardson, C. Alexander, S. Weygant, and P. F. Zhang, 2007: Dual-Doppler and single-Doppler analysis of a tornadic storm undergoing mergers and repeated tornadogenesis. *Mon. Wea. Rev.*, **135**, 736–758.

Wurman, J., J. M. Straka, E. N. Rasmussen, M. Randall, and A. Zahrai, 1997: Design and deployment of a portable, pencil-beam, pulsed, 3-cm Doppler radar. *J. Atmos. Oceanic Technol.*, **14**, 1502–1512.